Acta Cryst. (1996). D**52**, 176–188

Three-Dimensional Structure of *Xenopus laevis* Cu,Zn Superoxide Dismutase *b* Determined by X-ray Crystallography at 1.5 Å Resolution

KRISTINA DJINOVIĆ CARUGO,[a]*† ANDREA BATTISTONI,[a] MARIA TERESA CARRÌ,[b] FABIO POLTICELLI,[b] ALESSANDRO DESIDERI,[c] GIUSEPPE ROTILIO,[b] ALESSANDRO CODA,[a] KEITH S.WILSON[d] AND MARTINO BOLOGNESI[a,e]

[a]*Dipartimento di Genetica e Microbiologia, Università di Pavia. Via Abbiategrasso 207, 27100 Pavia, Italy,* [b]*Dipartimento di Biologia, Università di Roma 'Tor Vergata', Via della Ricerca Scientifica, 00133 Roma, Italy,* [c]*Dipartimento di Chimica Organica e Biologica, Università di Messina, Salita Sperone, 98166 Messina, Italy,* [d]*European Molecular Biology Laboratory c/o DESY, Notkestrasse 85, 22603 Hamburg, Germany, and* [e]*IST Centro Biotecnologie Avanzate and Dipartimento di Fisica, Università di Genova, Viale Benedetto XV 10, 16132 Genova, Italy*

(Received 27 March 1995; accepted 9 June 1995)

Abstract

Xenopus laevis Cu,Zn superoxide dismutase (recombinant isoenzyme *b*) has been crystallized and the structure determined at 1.49 Å resolution. The crystals belong to space group $P2_12_12_1$, with cell constants $a = 73.33$, $b = 68.86$, $c = 59.73$ Å, and contain one dimeric molecule of M_r 32 000 per asymmetric unit. The structure was solved by molecular-replacement techniques using the semisynthetic Cu,Co bovine enzyme as search model, and refined by molecular dynamics with a crystallographic pseudo-energy term. During the final steps, positional and anisotropic thermal parameters of the atoms were refined. The *R* factor for the 49 209 unique reflections in the 10.0–1.49 Å resolution range is 0.104, for a model comprising 2023 protein atoms, two Cu^{2+}, two Zn^{2+}, and 353 water molecules. The overall temperature factor for the model, including solvent, is 20.3 $Å^2$, while the calculated r.m.s. coordinate error for the refined model is 0.036 Å. As suggested by the primary structure homology to any other known intracellular eukaryotic superoxide dismutase (> 50%), the typical structural scaffolding of flattened antiparallel eight-stranded β-barrel is well conserved in *X. laevis* Cu,Zn superoxide dismutase *b*, together with the coordination geometry of the metal centers in the active site. The higher thermal stability of the *bb X. laevis* superoxide dismutase homodimer, with respect to dimers involving the *a*-type isoenzyme subunit(s), can be related, on the basis of the high-resolution structure, to side-chain and solvent interactions centered on residue Tyr149, in both *b*-type subunits. The analysis of the overall solvent structure reveals a number of equivalent water molecule sites in the two subunits, and in homologous superoxide dismutase models. Their locations are discussed in detail and classified on the basis of their structural role.

1. Abbreviations

SOD, superoxide dismutase; X-SOD*b*, *Xenopus laevis* Cu,Zn superoxide dismutase isoenzyme *b*; X-SOD*b*:CN, cyanide inhibited *Xenopus laevis* Cu,Zn superoxide dismutase *b*; B-SOD, bovine Cu,Zn superoxide dismutase; Y-SOD, yeast Cu,Zn superoxide dismutase; BCo-SOD, semisynthetic bovine Cu,Co superoxide dismutase.

2. Introduction

Superoxide dismutases are ubiquitous metalloenzymes that catalyse the disproportionation of the toxic superoxide radical into oxygen and hydrogen peroxide. In aerobic organisms this reaction is considered to play an essential protective role against oxidative toxicity of the chain reactions initiated by the $O_2^{\cdot-}$ radical (Halliwell & Gutteridge, 1989). Three different superoxide dismutases are found in cells, characterized by either copper and zinc, or manganese, or iron as natural prosthetic groups. The distribution of the three types of superoxide dismutases in organisms is considered to be characteristic of the evolutionary origin of the organism and of the associated cell organelles. Cu,Zn SOD's are inherently stable enzymes, predominantly found in the cytoplasm of all eukaryotes and in some bacteria, as dimers of M_r 32 000 (Stallings *et al.*, 1987; Parker & Blake, 1988; Bannister, Bannister, Barra, Bond & Bossa, 1991). Bovine superoxide dismutase (B-SOD) is particularly stable, being active in 8 *M* urea (Fridovich, 1986); with a melting temperature higher than 353 K (Lepock, Frey & Hallewell, 1990; Roe *et al.*, 1988), B-SOD is more thermostable than many proteins from thermophilic organisms (Stellwagen & Wilgus, 1978).

Three-dimensional structures are known in detail for the (oxidized) Cu, Zn SOD from four different species, namely ox (Tainer, Getzoff, Beem, Richardson & Richardson, 1982), spinach (Kitagawa *et al.*, 1991), yeast (Djinović, Gatti *et al.*, 1992) and human

† Current address: EMBL, Meyerhofstrasse 1, 6900, Heidelberg, Germany.

(Parge, Hallewell & Tainer, 1992), together with the semisynthetic Cu,Co bovine SOD (Djinović, Coda *et al.*, 1992). The central structural core of the SOD subunit is a flattened Greek-key β-barrel motif consisting of eight antiparallel β-strands joined by three external loops (Fig. 1). The topology of the Greek-key motif can be described, as proposed by Hutchinson & Thornton (1993), as $(3,2)_2$.

The molecular fold of the dimeric enzyme is highly conserved throughout the phyla, with a substantial conservation of primary structure; amino-acid identity scores of about 35% are observed when distantly related (mammalian and prokaryotic) SOD sequences are compared (Getzoff, Tainer, Stempien, Bell & Hallewell, 1989; Bordo, Djinović & Bolognesi, 1994). The metal cluster forming the enzyme active site is composed of a Zn^{2+} ion, coordinated by three histidyl and one aspartyl residue (His61, His69, His78, Asp81), and by the catalytically active Cu^{2+} ion sharing one ligand (His61) with the Zn^{2+} ion, and coordinated by three additional histidyl residues (His44, His46, His118), as well as by one water molecule (Tainer *et al.*, 1982).

During the catalytic reaction of Cu,Zn SOD, the Cu^{2+} ion is cyclically reduced and oxidized during successive encounters with the superoxide substrate at the active site. In the first step an electron from one superoxide radical is donated to the catalytic center with the formation of molecular oxygen and of a Cu^{+} ion, which in turn donates one electron to a second superoxide radical to produce, together with two protons, hydrogen peroxide (Fielden *et al.*, 1974; Getzoff *et al.*, 1983; Banci *et al.*, 1994). The reaction catalyzed by the bovine erythrocyte Cu,Zn SOD is relatively independent on pH,

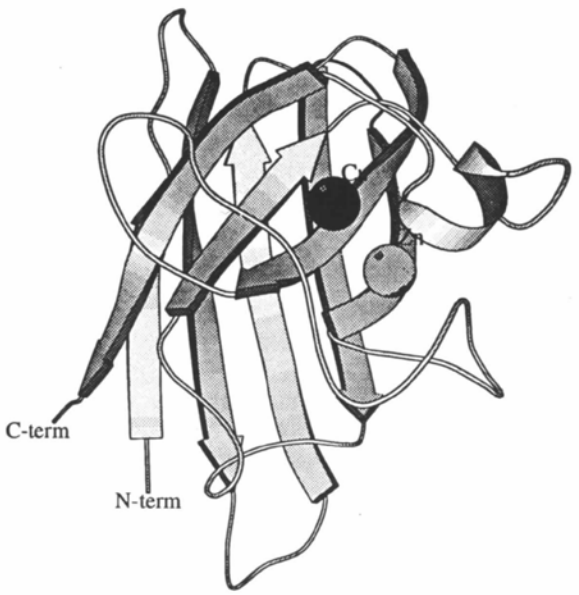

Fig. 1. Ribbon representation (Priestle, 1988) of *X. laevis* Cu,Zn superoxide dismutase *b* monomer. Active-site metal centers are drawn as solid spheres.

the reaction rate ($k = 3.9 \times 10^9\ M^{-1}\ s^{-1}$; O'Neill *et al.*, 1988) being in the range of typical diffusion-controlled reactions (Halliwell & Gutteridge, 1989; Sines, Allison & McCammon, 1990; Sergi, Ferrario, Polticelli, O'Neill & Desideri, 1996).

Electrostatic steering of the incoming $O_2^{\cdot-}$ substrate, by Cu,Zn SOD, is suggested by the salt dependence of the reaction rate, which decreases with increasing salt concentration (Cudd & Fridovich, 1982; Argese, Viglino, Rotilio, Scarpa & Rigo, 1987; O'Neill *et al.*, 1988). An enzyme–substrate recognition process based on electrostatic interactions has been proposed (Getzoff *et al.*, 1983), and supported by selective chemical modifications (Cudd & Fridovich; 1982; Argese *et al.*, 1987), by site-directed mutagenesis experiments, and simulations (Getzoff *et al.*, 1992; Banci, Bertini, Luchinat, Monnani & Scozzafava, 1988; Beyer, Fridovich, Mullenbach & Hallewell, 1987; Sines *et al.*, 1990; Fisher, Tainer, Pique & Getzoff, 1990; Polticelli *et al.*, 1995; Polticelli *et al.*, 1996). The overall kinetics of the process are dominated by diffusion of the negatively charged superoxide radical anion into the active-site channel, under control of the electrostatic charge distribution around the active site (Getzoff *et al.*, 1989, Desideri *et al.*, 1992 and references therein; Bordo *et al.*, 1994).

In the South African frog *Xenopus laevis*, a whole genome duplication, which occured approximately 30 million years ago (Bisbee, Beaker, Wilson, Hadji-Azini & Fishberg, 1977), is reflected by a high number of duplicated genes in each haploid genome. In fact, the sequence analysis of Cu,Zn SOD purified from *X. laevis* has indicated the presence of two isoenzymes with distinct amino-acid sequences (X-SOD*a* and X-SOD*b*) (Schininà *et al.*, 1989), different heat sensitivities and overall stability (Capo *et al.*, 1990). The more thermostable isoenzyme (X-SOD*b*) has been expressed in *Escherichia coli* (Battistoni, Carrì, Mazzetti & Rotilio, 1992), opening the way to the design of site-directed mutagenesis experiments on this protein (Polticelli *et al.*, 1995; Polticelli *et al.*, 1996). In this context, and in view of a more extended investigation on the structural bases of SOD catalytic activity and overall stability, we undertook the crystallographic analysis of recombinant X-SOD*b*, in parallel with functional studies of synthetic mutants (Polticelli *et al.*, 1995, 1996). The results of this investigation, together with the X-SOD*b* three-dimensional structure refined at 1.49 Å resolution, are reported in the present communication.

3. Materials and methods

3.1. *Crystallization, data collection and structure solution*

Crystals of X-SOD*b* were grown in the orthorhombic space group $P2_12_12_1$ with unit-cell parameters $a = 73.33$, $b = 68.86$, $c = 59.73$ Å, using sitting-drop vapour diffusion as described previously (Djinović Carugo *et al.*, 1993). Briefly, the protein stock solution (at a concen-

tration of 10 mg ml^{-1}) was added to an equal volume of crystallization medium containing 18%(*w*/*v*) of polyethylene glycol (M_r = 4000), 0.05 *M* sodium phosphate (pH 6.0). Crystals with dimensions of 0.2 × 0.1 × 0.8 mm grew in 6 weeks at 301 K. The calculated packing density parameter V_M (Matthews, 1968) is 2.34 Å^3 Da^{-1}, assuming one dimer (32 000 kDa) per asymmetric unit.

X-ray diffraction data, to a resolution limit of 3.0 Å were preliminary collected at room temperature on an image-plate area-detector system (MAR Research, Germany), installed on a Rigaku RU200 rotating-anode generator. Subsequently, a new data set of X-ray intensities (up to 1.49 Å) was collected using the EMBL X31 synchrotron radiation source beamline at the DORIS storage ring c/o DESY, Hamburg, employing a locally developed image-plate system as detector (J. Hendrix & A. Lentfer, unpublished results) and a wavelength of 0.92 Å. Oscillation ranges were set at the angle subtended by the crystal cell dimensions in order to avoid spatial overlap of recorded reflections (Arndt & Wonacott, 1977). Two low-resolution passes (at 2.39 and 3.44 Å) were needed to measure reflections saturated during the longer collection times used in the high resolution pass. All three data sets were collected from a single crystal of dimensions 0.25 × 0.10 × 0.65 mm at 277 K.

Refinement of orientation and integration of the intensities was performed using the *MOSFLM* suite of programs (Leslie, 1986). Merging of the observed intensities into a unique data set of reflections was carried out using *ROTAVATA/AGROVATA* programs from the *CCP*4 suite (Collaborative Comptational Project, Number 4, 1994) and the intensities converted to structure-factor amplitudes using the program *TRUNCATE* (French & Wilson, 1978). 245 181 measurements were merged to yield 49 209 unique reflections (98.8% of the theoretical reflections in the to 1.49 Å resolution range). The merging R_m factor ($R_m = \sum|I_i - \langle I\rangle|/\sum|I_i|$, where I_i is the intensity of an observation, $\langle I\rangle$ is the mean intensity value of the reflection, and the summations are over all reflections) was 0.078.

The structure was first solved using the data set collected to 3.0 Å resolution (Djinović Carugo *et al.*, 1993) by molecular replacement, employing semisynthetic bovine Cu,Co bovine SOD (Djinović, Coda *et al.*, 1992) as a search model. The initial *R*-factor value for the diffraction data in the 15.0–3.0 Å shell was 0.412.

3.2. *Refinement of the three-dimensional atomic model*

In the first step the atomic model was refined with the diffraction data at 3.0 Å resolution using the simulated-annealing and energy-minimization protocols implemented in *X-PLOR* (Brünger, 1992*a*), with bond length and angle parameters derived from the Cambridge Database of model structures (Engh & Huber, 1991). The conventional *R* factor at the end of this refinement was 0.189, in the 6.0–3.0 Å resolution range. When the synchrotron data set was available, the resolution was gradually increased to 1.6 Å; the *X-PLOR* refinement converged to a *R*-factor value of 0.234, and free *R* factor of 0.287 (calculated on 10% of the data set; Brünger, 1992*b*) for the diffraction data in the 6.0 to 1.6 Å resolution range.

The refinement was continued with restrained techniques using the *PROLSQ* program suite (Konnert & Hendrickson, 1980), in combination with the program *ARP* (Lamzin & Wilson, 1993) for automatic search of solvent molecules in the model, and alternated with inspections of model/electron-density maps with *FRODO* (Jones, 1978). During the refinement geometrical constraints to the copper and zinc coordination spheres were applied, adopting metal–ligand distances observed in small molecules coordination chemistry (Orpen *et al.*, 1989). When the inspection of the electron-density maps and convergence of the *R* factor (0.150 in the 10.0–1.49 Å resolution range) indicated that no major errors were left in the model, non-polar H-atom positions were calculated and included in the refinement as fixed-atom contribution. This procedure additionally lowered the crystallographic *R* factor to 0.145 (R_{free} = 0.178) and improved the mean bond distances which tended to be systematically longer before explicit inclusion of H atoms in the model.

At this stage refinement of positional and of anisotropic thermal parameters of non-H atoms was performed using *SHELXL*93 (Sheldrick, 1993). Bond length and angle parameters used were those of Engh & Huber (1991). The validity of the anisothropic temperature-factor refinement was checked by means of the Hamilton test (Hamilton, 1965), and by continuous monitoring of the free *R* factor, which dropped from 0.178 to 0.169. During this part of the refinement all metal–ligand restraints were released. The inspection of electron-density maps with coefficients ($2|F_o| - |F_c|$) and ($|F_o| - |F_c|$), and calculated phases, allowed additional modelling of ordered solvent structure and of alternate conformations for 15 side chains in the asymmetric unit.

4. Results and discussion

4.1. *General properties of the refined model*

The final *R* factor calculated for the X-SOD*b** dimer model (2023 protein atoms, two Cu^{2+}, two Zn^{2+} ions and 353 ordered solvent molecules) is 0.104 for all reflections, 0.096 for $|F_o| > 4\sigma(|F_o|)$, and the goodness of fit† is 0.905. The features in the final difference

* Atomic coordinates and structure factors have been deposited with the Protein Data Bank, Brookhaven National Laboratory (Reference: 1XSO, R1XSOSF). Free copies may be obtained through The Managing Editor, International Union of Crystallography, 5 Abbey Square, Chester CH1 2HU, England (Reference: JN0014).

† Goodness of fit = $\sum(|F_o| - |F_c|)^2$/(No. of reflections − No. of parameters).

electron-density map are within 0.41 and -0.27 e Å^{-3}. Deviations from ideal stereochemical parameters are 0.020 Å for bond angles, 0.029 Å for angle distances, and 0.044 Å for planar 1–4 distances. Inspection of the Ramachandran plot (Ramakrishnan & Ramachandran, 1965) of the whole dimer shows only two residues, Asp24 in both X-SOD*b* crystallographically independent subunits, in non-allowed φ,ψ regions. Moreover, assessment of the structure quality, as provided by the program *PROCHECK*, shows better than average figures for all the reliability indices tested (Laskowski, MacArthur, Moss & Thornton, 1993). These observations are substantiated by the analysis of the final results by means of the σ_A method (Read, 1986), from which an r.m.s. coordinate error of 0.036 Å can be derived.

As suggested by the substantial degree of primary-structure homology [X-SOD*b* shares more that 50% residue identities with all other known intracellular eukaryotic SOD's (Bordo *et al.*, 1994)], the typical tertiary and quaternary structures of SOD's are well conserved in the X-SOD*b* variant here examined (see Fig. 1). Overlays of X-SOD*b* dimeric Cα backbones with BCo-SOD (Djinović, Coda *et al*, 1992) and Y-SOD (Djinović, Gatti *et al.*, 1992) yield r.m.s. deviations of 0.726 and 1.170 Å, respectively. The two X-SOD*b* subunits (Cα backbones) overlay with an r.m.s. deviation of 0.359 Å, very close to the 0.323 Å r.m.s. deviation observed in the comparison of the unhinibited X-SOD*b* dimer structure with that of the X-SOD*b*:CN complex, which has been studied at 98 K (Djinović Carugo *et al.*, 1994).

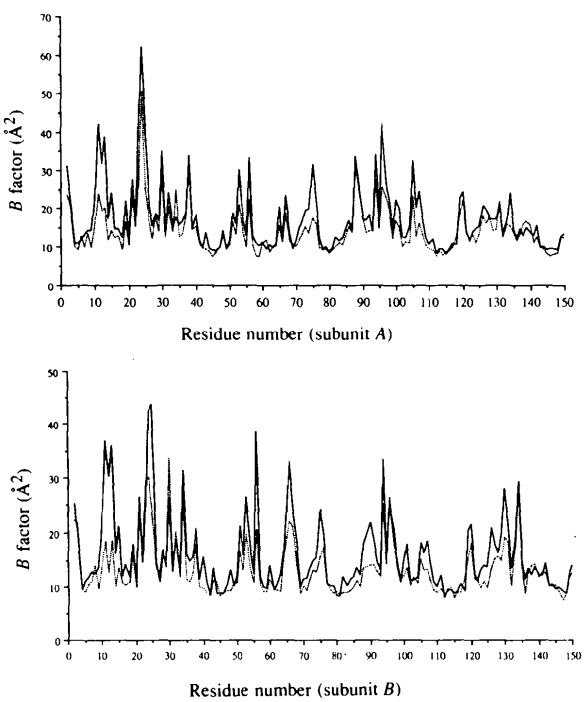

Fig. 2. (*a*) Plot of average *B* factors, per residue, for both subunits of X-SOD*b* (continous line) and X-SOD*b*:CN complex (dotted line).

Table 1. *Secondary-structure assignment of X-SODb*

Defined by *DSSP* (Kabsch & Sander, 1983). Loop regions and corresponding names are as referred to in the text.

β-strands		Loop regions	
Residue No.	Name	Residue No.	Name
4–8	1*a*	9–14	I
15–22	2*b*	23–26	II
27–34	3*c*	35–38	III
39–46	6*d*	47–80	IV
81–87	5*e*	88–91	V
92–99	4*f*	100–113	VI Greek-key loop
114–118	7*g*	119–140	VII Electrostatic channel loop
141–149	8*h*		

The average *B* factor for the protein atoms is 17.1 and 42.7 Å^2 for solvent molecules, while the overall temperature factor of the model including ordered solvent, is 20.3 Å^2. The per-residue temperature-factor profiles for both X-SOD*b* subunits correlate with the location of β-strands within the SOD Greek-key motif, and with the *B*-factor profiles of other known SOD structures. Table 1 shows the secondary-structure assignment of X-SOD*b*. Fig. 2 shows the per-residue temperature-factor profile of the uninhibited X-SOD*b*, and of the low-temperature structure of the X-SOD*b*:cyanide complex (Djinović Carugo *et al.*, 1994), which displays an average *B* factor for the protein atoms of 13.9 Å^2 (30.3 Å^2 for solvent molecules). Allowing for an overall relative temperature rescaling of the two independent experimental results, the agreement between the two sets is quite satisfactory. The difference between overall protein temperature factors in X-SOD*b* and its cyanide complex crystal structure is 3.2 Å^2; if the average *B* factors of residues building up the homodimer interface are compared, a smaller variation (11.5 and 10.1 Å^2 for X-SOD*b* and X-SOD*b*:CN complex, respectively) is observed, in keeping with the tight packing and structural stability of this region of the protein even at 277 K. Similarly, several residues contributing to the intermolecular crystal contacts in one subunit show lower temperature factors with respect to the same residues not contributing to crystal lattice formation in the other SOD subunit.

4.2. *Structural variability of X-SODb*

The less conservative amino-acid substitutions of X-SOD*b*, with respect to B-SOD, taken as the reference molecule in this protein family, can be divided into two classes: (*a*) those altering the residue size or polarity; (*b*) those affecting Gly or Pro residues. The first class includes the following major amino-acid substitutions (B-SOD to X-SOD*b*): Asp40Leu, Thr56Met, Leu65Glu, Met115Ala. Leu40 in the 6*d* β-strand, and Glu65, in loop IV, are solvent-exposed residues in X-SOD*b* (solvent-accessible surface areas: Leu40, 87 and 90 Å^2 in subunits *A* and *B*, respectively; Glu65, 88 and 119 Å^2 in subunits

A and *B*, respectively), and do not pose constraints on the local protein conformation, if compared with other SOD models. The Thr56Met substitution, also, occurs at the enzyme surface (the Met56 solvent-accessible area is 114 and 121 Å^2 in subunits *A* and *B*, respectively), and does not affect the protein backbone significantly. Nevertheless, a substitution at this site is considered of interest since the methionyl residue is in contact, through the SD atom, with the side chain of the catalytic residue Arg141 (Met56 SD···Arg141 CD distances are 3.64 and 3.86 Å in subunits *A* and *B*, respectively). Although site 56 is fairly exposed to the solvent, the occurrence of a methionyl residue is rather common in plant SOD. Despite the larger size of Met, as compared to the Thr residue common in higher vertebrates, no steric hindrance on the correct positioning of Arg141 side chain is observed in the X-SOD*b* active site.

The β-barrel core replacement of Met115, observed in B-SOD, with Ala, results in a conformational readjustment, in X-SOD*b*, of Phe43, which is a highly conserved residue and provides hydrophobic packing across the β-barrel core. Due to the decreased volume of residue 115 and to the concurrent Ile18Val substitution, two residues in this inner region of the protein, Cys6 and Leu8, have enough room to adopt alternate conformations for their side chains. The Val45Ile substitution, again occurring close to residue Ala115, may be required to avoid loss of core hydrophobic interactions. Such a substitution with a bulkier residue, at site 45, may also prevent conformational flexibility of the polypeptide backbone at flanking residues His44 and His46, which are active site Cu^{2+} ligands.

Table 2 lists the alternate side-chain conformations observed for 15 residues in the X-SOD*b* dimer. Besides those referring to Cys6 and Leu8, discussed above, most of the alternate conformations are observed at surface residues, and are equally found in both X-SOD*b* subunits.Thus, they reflect a more general structural feature, which is highlighted in X-SOD*b* by the high experimental resolution achieved. Residue Asn51, which is close to the dimer interface, forms with its O, C and CB atoms van der Waals interactions with side-chain atoms of residue Val7 from the facing subunit. The intersubunit contacts are therefore achieved through atoms of Asn51 whose positions are not affected by the observed alternate side-chain conformations (see Table 2).

Among amino-acid substitutions belonging to the second class described above, at the beginning of the 2*b* β-strand Asp13 substitutes for the prolyl residue common in higher vertebrate SOD's. The substitution site is at a sharp corner of a five-residue turn, and can accommodate Glu or Gly residues in lower phyla SOD's. Despite the increased polarity brought about by Asp13, the solvent structure in the close neighbourhood of the polypeptide chain is conserved with respect to B-SOD and Y-SOD. Water molecules W33 and W155 in subunit *A*, and W36 and W101 in subunit *B* are hydrogen bonded to the backbone atoms of residues Gly10, Gly12, Val14, and Leu142, the distances ranging from 2.67 to 3.31 Å. The rigid solvent structure trapped in this five-residue turn links it by means of the hydrogen-bonding network to the N-terminal part of the β-strand 8*h* (position 142), achieving local stabilization of the protein structure.

Table 2. *Residues for which alternate side-chain conformations have been located in X-SODb subunits A and B*

Residue	Chain	Residue	Chain
Cys6	*A*	Cys6	*B*
Leu8	*A*	Leu8	*B*
Ser28	*A*	Ser28	*B*
Asn51	*A*	Asn51	*B*
Ser60	*A*	—	—
—		Val92	*B*
Ser100	*A*	Ser100	*B*
—		Ser103	*B*
Ser150	*A*	Ser150	*B*

The single-residue insertion of X-SOD*b* occurs, at site 25A (Gly); the polypeptide backbone conformation observed at this site can be classified as a type-II′ β-turn. Inspection of the refined structure shows that the Gly25A insertion has a very limited effect on the course of the neighbouring β-strands, in the SOD tertiary structure. In the neighbouring region of the molecule the side chain of the strongly conserved residue Gln22 forms hydrogen bonds to main-chain N atoms of residue Leu104 (2.93 and 2.88 Å in subunits *A* and *B*, respectively), and to Ser103 atom (3.39 and 3.29 in subunits *A* and *B*, respectively). These interactions link this part of the structure to the body of the protein scaffolding, and suggest the reason for strong residue conservation at position 22 in the SOD family. Additionally, in subunit *B*, a hydrogen bond of 3.16 Å is observed between Lys105 NZ (a basic residue occurring in this position only in X-SOD) and the Gln22 OE1 atom.

Residue Gly90 substitutes for Asn in B-SOD. The polypeptide backbone conformation in this region of X-SOD is substantially altered with respect to other enzyme structures, due to the deletion of one residue. On the basis of overlayed three-dimensional structures, the deleted residue can be properly located at site 89, thus assigning the 88 position to a Glu residue in X-SOD*b*. The perturbed structure of the 89–92 turn is shown in Fig. 3, where the location of residue Val92 is shown. In the *B* subunit of X-SOD*b* Val92 has two alternate conformations (see Table 2). In the second electrostatic shell of the enzyme a Pro residue of B-SOD is substituted by Ala at site 121 without affecting the structure of this functionally relevant area. Similarly all the other Pro or Gly substitutions occurring in X-SOD*b* (listed in Table 3) have no clear effect on the polypeptide backbone local conformation.

Table 3. *Substitutions of Gly or Pro residues in B-SOD amino-acid sequence with respect to X-SODb*

B-SOD	X-SOD*b*
Pro13	Asp13
Gly24	Asp24
Pro60	Ser60
Gly71	Ala71
Lys73	Gly73
Asn90	Gly90
Pro100	Ser100
Glu107	Pro107
Ser140	Gly140
Lys151	Pro151

The presence of an aromatic residue at site 149 is rather uncommon in SOD sequences, and, besides *X. laevis*, it is only found in the blood fluke extracellular SOD (Simurda, van Keulen, Rekosh & Lo Verde, 1988). The aromatic ring of Tyr149, in X-SOD*b*, provides an intermolecular contact between the dimer subunits, making use of the Arg113 guanidino group of the contacting monomer. As shown in Fig. 4, the guanidinium end of Arg113 in subunit *A*, is sandwiched between Phe62 from the same subunit and Tyr149 belonging to subunit *B*. This interaction, due to the almost exact twofold axis at the subunit interface, occurs twice in the active dimer. Site 149 has been recognised as a contributing residue to dimer formation, through main-chain–main-chain hydrogen bonds to Gly49 and Gly112 residues in all known SOD structures. Indeed these main-chain interactions are also observed at the dimer interface in X-SOD*b*.

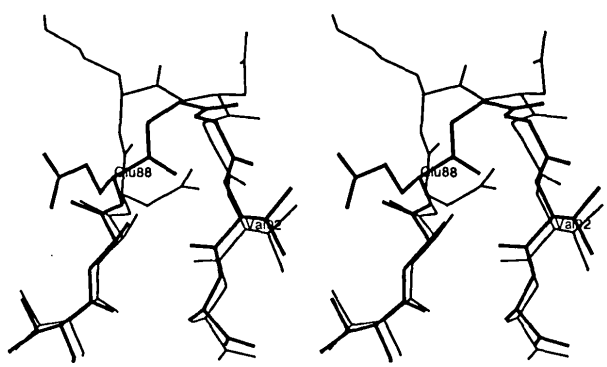

Fig. 3. Comparison of β-turn conformations, hosting a one-residue deletion at position 89 (X-SOD*b*, bold line; BCo-SOD, thin line; subunit *A* shown).

4.3. *X-SOD isoenzymes and dimer stability*

Sequence analysis of Cu,Zn SOD isolated from *X. laevis* showed the presence of two different polypeptide chains, representing the translation products of duplicated genes X-SODa and X-SOD*b* (Schininà *et al.*, 1989). On this basis, three isozymes, corresponding to *aa*, *ab* and *bb* dimer subunit compositions have been identified, showing the same molecular weight and isoelectric point (p*I* = 4.65) at acidic pH (Capo *et al.*, 1990). On the other hand, above neutrality, the three forms migrate differently in an electrophoretic field, the *bb* dimer giving the most anodic electromorph. Such behaviour, in view of the 20 amino-acid differences between the *aa* and *bb* X-SOD isozymes, is in keeping with the substitution of Arg19, of the *a*-type chain, with His in the *b*-type chain. His19 is highly exposed to solvent in both X-SOD*b* subunits (85 and 91 Å^2, in subunits *A* and *B*, respectively), and located in the central part of β-strand 2*b*, as a surface residue. Its ionization, expected near neutrality for a solvent exposed histidine, accounts for the achievement of the same net charge at acidic pH in the *aa* as well as in the *bb* dimers, whose net charges at alkaline pH differ by one unit.

Although heterodimeric X-SOD may occur *in vivo* (Capo *et al.*, 1990), its segregation into homodimers is favoured by heat treatment or by standing in solution for long times, suggesting slightly more favourable interactions for dimer formation at the homodimer subunit interface (Capo *et al.*, 1990). As suggested by subunit interchange experiments run on several SOD's from different species (Tegelstrom, 1975), the dimer interface is highly conserved in shape and (*a*) polarity, this being also true for X-SOD. A closer look at the refined X-SOD*b* structure, and consideration of the amino-acid

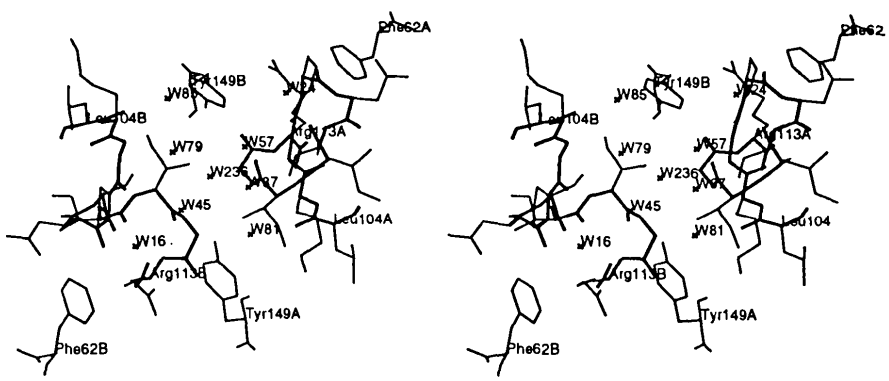

Fig. 4. Stereoscopic drawing presenting the surface cleft at the dimer interface between the two X-SOD*b* subunits. The aromatic stacking between residues Tyr149 from subunit *A* with Arg113 and Phe62 from subunit *B* is formed twice due to the molecular twofold axis located approximately on water molecule W236. The solvent structure centered on W236, which contributes to inter-subunit interactions is also shown.

differences characterising X-SOD*a* with respect to the *b*-isozyme, show that the Phe–Cys 149–150 interface residues (in *a*-type) are replaced by Tyr–Ser in the *b*-type. Residue 149 is accommodated in a narrow cleft, neighboring residues 104–107 of subunit *A*, and residues 110–113 of subunit *B*. Tyr149 OH hydroxyl is located at the entrance of this cleft, and forms part of a tight hydrogen-bonding network (see Fig. 4, and discussion above) built up by donors/acceptors from both subunits and by ordered water molecules. Among these, water molecule W45 bridges the Tyr149 OH atom (3.12 Å) of subunit *A*, and the main-chain carbonyl O atom of Leu111 (2.70 Å) of subunit *B*. Due to the local twofold axis relating the two polypeptide chains of the dimer, an analogous interaction is mediated by solvent molecule W57 and Tyr149 OH from subunit *B* (3.03 Å) and Leu111 O atom from subnit *A* (2.69 Å). It is expected that upon replacement of Tyr149 with Phe (in X-SOD*a*) the solvent structure and interactions in this area will be perturbed to a significant extent, deleting solvent-mediated subunit interactions in this area.

A similar structural arrangement is observed in the neighborhood of residue 150, which is in a surface cleft between residue 3 (from the *A* subunit) and residue 50 (from the *B* subunit), and surrounded by several ordered water molecules. Nevertheless, no conclusions can be drawn on the potential dimer-stabilizing interactions achieved by this residue (either Cys or Ser, in *a*-type and *b*-type X-SOD, respectively), due to its alternate conformations and to the conserved hydrogen-bonding capabilities (although not entirely comparable) of the side chains in both structures.

In contrast, the presence of a seryl residue at position 150, as opposed to Cys, can be related to the higher thermal stability of the *b*-type X-SOD homodimer, with respect to the *a*-type, shown by enzyme inactivation tests at 343 K (Capo *et al.*, 1990). Indeed, the presence of free thiols in the *a*-type homodimer can increase the rate of temperature-induced irreversible denaturation, as observed in the heat-inactivation experiments of the Cys6Ala mutant of B-SOD (McRee *et al.*, 1990) as well as Cys6Ala and Cys109Ser mutants in human SOD (Lepock, Frey & Hallewell, 1990).

4.4. *X-SODb active-site structure*

The coordination sphere of the copper ion consists of four conserved histidines (liganding atoms His44 ND1, His46 NE2, His61 NE2, and His118 NE2); the zinc ion is liganded to three histidines and one aspartate residue (atoms ND1 of the three histidines at positions 61, 69, 78, and OD1 atom of Asp81). As observed in bovine (Tainer *et al.*, 1982), spinach (Kitagawa *et al.*, 1991) and yeast SOD's (Djinović, Gatti *et al.*, 1992), the bridging ligand His61 defines a plane which approximately contains both metal ions at a distance of about 6 Å. The zinc coordination geometry is distorted

Table 4. *Coordination distances and angles*

(*a*) Coordination distances (Å) for the Cu^{2+} and Zn^{2+} centers in the *A* and *B* subunits of X-SOD*b*, BCo-SOD (Djinovic, Coda *et al.*, 1992) and of B-SOD (Tainer *et al.*, 1982).

Cu^{2+}	X-SOD*b*		BCo-SOD		B-SOD	
	A	*B*	*A*	*B*	*A*	*B*
His44 ND1	2.00	1.97	2.09	2.02	2.01	1.96
His46 NE2	2.21	2.17	2.29	2.18	2.11	2.12
His61 NE2	2.08	2.08	2.16	1.99	2.21	1.98
His118 NE2	2.11	2.07	2.13	2.14	2.09	1.99
Water	2.26	2.48	2.38	2.89	3.0	
Zn^{2+}/Co^{2+}	X-SOD*b*		BCo-SOD		B-SOD	
	A	*B*	*A*	*B*	*A*	*B*
His61 ND1	2.04	2.02	2.11	1.99	2.09	2.07
His69 ND1	2.07	2.04	2.01	2.32	2.14	2.08
His78 ND1	2.06	2.00	2.02	1.97	2.04	2.16
Asp81 OD1	2.00	1.97	1.99	1.96	1.91	2.07

(*b*) Angles (°) around the copper ion as observed in the X-SOD*b*, for *A* and *B* subunits.

				A	*B*
His44 ND1	Cu^{2+}	His61	NE2	87.1	87.0
His61 NE2	Cu^{2+}	His46	NE2	90.5	92.4
His46 NE2	Cu^{2+}	His118	NE2	99.9	98.2
His118 NE2	Cu^{2+}	His44	ND1	90.6	91.1
Water	Cu^{2+}	His44	ND1	118.8	125.4
Water	Cu^{2+}	His46	NE2	100.6	95.1
Water	Cu^{2+}	His61	NE2	82.4	80.7
Water	Cu^{2+}	His118	NE2	87.3	89.2

tetrahedral, whereas copper, previously considered in a distorted square planar coordination, is more properly described by a trigonal bipyramidal coordination considering His44 ND1, His46 NE2 and the water molecule as equatorial ligands.

Table 4 presents metal coordination distances at the active site as observed in X-SOD*b*, B-SOD and BCo-SOD. The metal–ligand distances as well as the coordination geometries are strictly conserved in the two X-SOD*b* subunits, as well as in all crystal structures taken into consideration. Additionally, a solvent molecule observed in SOD structures at the fifth coordination site of copper ion, is found in the X-SOD*b* at shorter coordination distances than in other known cases. These values are in good agreement with EXAFS studies on the native bovine enzyme (Blackburn, Strange, McFadden & Hasnain, 1987), where the solvent molecule was observed at 2.25 Å from the copper ion. Similarly, in the crystal structure X-SOD*b*:CN adduct the inhibitor was located at 2.20 and 2.28 Å (in subunits *A* and *B*, respectively) from the catalytic copper ion (Djinović Carugo *et al.*, 1994).

In the active-site region the side chain of Asp122 acts as a bridge between His44 (copper ligand) and His69 (zinc ligand) forming hydrogen bonds with histidyl side chains of each of these two metal-liganding residues and defining their correct mutual orientation. In detail, Asp122 OD1 atom is surrounded by two H-atom donors, His69 NE2 and Leu124 N atoms at distances of 2.76 and

2.80, 2.80 and 2.79 Å, respectively (in subunits *A* and *B*), while Asp122 OD2 interacts with His44 NE2 and His69 NE2 (2.67 and 2.69, 3.10 and 3.11 Å, in subunits *A* and *B*, respectively). In this context it is noticeable that the Asp122 OD11···Leu122 N hydrogen bond is favoured by the left-handed α-helical conformation of Leu124. These interactions, which are relevant for the active-site structural organization, are conserved in the other known SOD three-dimensional structures (Bordo *et al.*, 1994). Moreover, hydrogen-bonding interactions involving water molecules in the active site are also substantially conserved, as compared to BCo-SOD as well as Y-SOD (Djinović, Coda *et al.*, 1992; Djinović, Gatti *et al.*, 1992), and are discussed below.

The putative entrance to the active-site channel is defined by the lower and upper rims of the protein structure, formed by residues at positions 56, 58–60, 63, and 130–131, 134–139, 141, respectively (Getzoff *et al.*, 1983). Residue Thr135 narrows the active-site channel, and the positively charged guanidinium group of Arg141 (strictly conserved in SOD's) guides the substrate toward the catalytic Cu^{2+} coordination site, stabilizing the bound superoxide ion (see Fig. 5).

4.5. *Solvent structure*

The high-resolution refinement here reported for the oxidized free enzyme (data collected at 277 K) along with the availability of the refined structure of the X-SOD*b*:CN complex (data collected at 98 K, to 1.7 Å resolution) allow us to examine details of the solvent structure, in the same protein, under different experimental conditions.

As already mentioned, the X-SOD*b* model contains 353 solvent molecules with an average *B* factor of 42.7 Å^2, while 498 water molecules with a mean temperature factor of 30.3 Å^2 were located during the refinement of X-SOD*b*:CN crystal structure. The comparison of the hydrogen-bonding interactions of solvent molecules as observed in the two crystal structures is summarized in Table 5. As expected, the number of protein-bound ordered water molecules in all classes is systematically higher in the X-SOD*b*:CN low-temperature crystal structure than in the X-SOD*b* refined model. Additionally, the mean hydrogen-bonding distances, for all classes, are shorter in the X-SOD*b*:cyanide model with respect to X-SOD*b*. This is in line with the results of X-ray crystallographic studies of the ribonuclease A [at nine different temperatures between 98 and 320 K (Tilton, Dewan & Petsko, 1992)], where a general decrease in distances for hydrogen-bonding interactions was observed upon lowering the data-collection temperature.

After least-squares superpositions of X-SOD*b* and X-SOD*b*:CN dimer Cα backbones, 65 water molecules are found at sites which are within 0.323 Å from each other (the r.m.s. deviation of the comparison), indicating negligible influence of ionic strength and temperature on their locations with respect to the protein and crystalline lattice.

In contrast, analysis of solvent structure in the two crystallographically independent X-SOD*b* subunits showed 77 water molecule pairs located within the

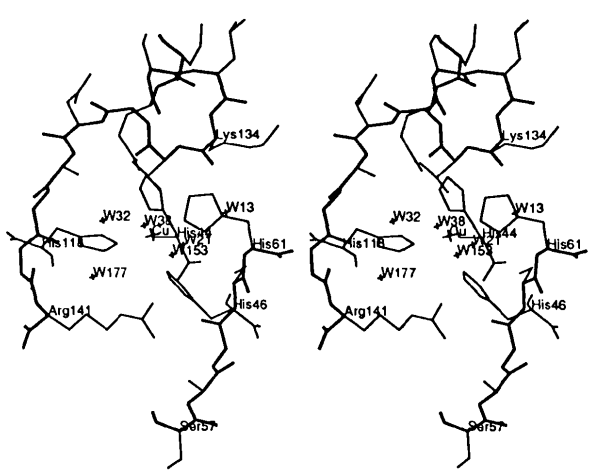

Fig. 5. Stereoscopic view of the X-SOD*b* active site (in subunit *A*), along with the upper and lower rim residues, forming the active-site channel (bold backbone segments respectively on the left and the right sides of the figure). The conserved solvent molecules filling this channel, and forming the hydrogen-bonding network, are also shown.

Table 5. *Statistics on solvent structure as observed in the XSODb and X-SODb:CN complex (XCN) models*

A hydrogen-bond cutoff distance of 3.5 Å was used throughout, together with angular cutoff values of 120 and 90° (as minimum acceptable values) at the H and O atoms, respectively. Program *CONTACT*, Collaborative Computational Project, Number 4 (1994).

	X-SOD*b*	B_{av} (Å^2)	X-SOD*b*:CN	B_{av} (Å^2)
No. H_2O in the model	353	43	496	30
No. H_2O forming 1 hydrogen-bond	44	53	33	39
No. H_2O forming 2 hydrogen-bonds	79	48	98	37
No. H_2O forming 3 hydrogen-bonds	101	41	166	30
No. H_2O forming 4 hydrogen-bonds	119	35	197	25
No. H_2O forming 0 hydrogen-bonds to protein	2	54	2	27
No. H_2O forming 1 hydrogen-bond to protein	47	52	33	39
No. H_2O forming 2 hydrogen-bonds to protein	79	47	99	37
No. H_2O forming 3 hydrogen-bonds to protein	98	42	166	30
No. H_2O forming 4 hydrogen-bonds to protein	119	35	196	25

	X-SOD*b*			X-SOD*b*:CN		
Hydrogen-bond type	No.	d_{av} (Å)	B_{av} (Å^2)	No.	d_{av} (Å)	B_{av} (Å^2)
Main-chain O···H_2O	183	2.95	37.1	220	2.92	26.4
Main-chain N···H_2O	77	3.01	31.8	90	2.96	20.6
Side-chain O···H_2O	667	2.92	41.5	1143	2.88	29.6
Side-chain N···H_2O	48	3.00	42.2	60	2.97	30.7

Table 6. *Buried solvent molecules equivalently located in subunits A and B, of X-SODb, and their hydrogen-bonding interactions*

	Subunit *A*					Subunit *B*			
	Atom	Residue		Distance (Å)		Atom	Residue		Distance (Å)
W2	N	Val *A*	7	2.97	W4	N	Val *B*	7	2.97
	O	Val *A*	146	2.72		O	Val *B*	146	2.69
	OH	W	5	2.84		OH	W	8	2.87
	OH	W	100	2.91		OH	W	145	2.86
W8	N	Asn *A*	51	2.99	W5	N	Asn *B*	51	2.94
	O	Gly *A*	49	2.89		O	Gly *B*	49	2.91
	OH	W	4	2.87		OH	W	2	2.84
W3	OD1	Asn *A*	63	2.70	W6	OD1	Asn *B*	63	2.77
	N	Glu *A*	65	2.98		N	Glu *B*	65	3.17
	N	Val *A*	79	3.15		N	Val *B*	79	3.25
	OH	W	12	2.71		OH	W	14	2.74
W9	O	Gly *A*	70	2.86	W7	O	Gly *B*	70	2.93
	N	Gly *A*	83	3.06		N	Gly *B*	83	3.01
	OD2	Asp *A*	122	2.79		OD1	Asp *B*	122	2.78
W38	CU	Het *C*	1	2.26	W10	CU	Het *C*	3	2.40
	OH	W	235	2.09		OH	W	25	2.73
	OH	W	32	2.91		OH	W	30	2.92
	OH	W	21	3.14		OH	W	1	1.61
W13	N	His *A*	61	3.06	W11	N	His *B*	61	3.06
	O	Lys *A*	134	2.84		O	Lys *B*	134	2.80
	OH	W	21	3.01		OH	W	25	2.91
	OH	W	232	2.86		OH	W	200	3.13
W12*	O	Arg *A*	77	2.77	W14*	O	Arg *B*	77	2.84
	OH	W	3	2.71		OH	W	6	2.74
	OH	W	99	2.85		OH	W	53	2.90
W24	O	Pro *A*	107	2.97	W16	O	Pro *B*	107	2.84
	O	Ser *A*	109	2.73		O	Ser *B*	109	2.79
	NH1	Arg *A*	113	2.98		NH1	Arg *B*	113	2.97
	OH	W	300	2.67					
W25	OH	W	10	2.73	W21	OH	W	38	3.14
	OH	W	317	2.64		OH	W	235	2.61
	OH	W	11	2.91		OH	W	153	2.72
	OH	W	351	3.46		OH	W	13	3.01
W17	N	Asn *A*	63	2.85	W23	N	Asn *B*	63	2.86
	OH	W	150	2.67		OH	W	250	2.73
	OH	W	309	2.19		OH	W	288	2.69
W32	O	Gly *A*	139	2.87	W30	O	Gly *B*	139	2.88
	OH	W	38	2.91		OH	W	10	2.92
	OH	W	235	2.49		OH	W	72	3.14
	OH	W	131	3.16		OH	W	1	2.95
W31	N	Thr *A*	37	2.91	W34	OG1	Thr *B*	37	3.33
	OG1	Thr *A*	37	3.24		N	Thr *B*	37	2.98
	OH	W	89	2.82		OH	W	74	2.86
	OH	W	159	2.27		OH	W	148	2.62
W33	N	Gly *A*	10	2.93	W36	N	Gly *B*	10	2.99
	O	Gly *A*	10	3.20		O	Gly *B*	10	3.48
	O	Gly *A*	12	2.68		O	Gly *B*	12	2.98
	O	Val *A*	14	2.74		O	Val *B*	14	2.68
W83	N	Leu *A*	40	2.98	W43	N	Leu *B*	40	2.90
	OH	W	187	3.16		OH	W	256	3.35
	OH	W	329	2.72		OH	W	28	3.34
						OH	W	297	3.14
W63	O	His *A*	19	3.37	W50	O	His *B*	19	3.38
	O	Ser *A*	28	3.05		O	Ser *B*	28	3.16
	OH	W	240	3.21		OH	W	203	3.23
W45	O	Ile *B*	111	2.70	W57	O	Ile *A*	111	2.69
	OH	Tyr *A*	149	3.13		OH	Tyr *B*	149	3.03
	OH	W	236	2.62		OG	Ser *A*	109	3.39
	OH	W	79	3.49		OH	W	236	2.80
W126	N	Ser *A*	11	3.08	W65	OG	Ser *B*	11	3.47
	OG	Ser *A*	11	2.35		N	Ser *B*	11	3.03
	O	Arg *A*	141	3.09		O	Arg *B*	141	3.10
	O	Leu *A*	142	3.34		O	Leu *B*	142	3.28
	OH	W	152	2.91		OH	W	93	2.82

Table 6 (*cont.*)

	Subunit *A*					Subunit *B*			
	Atom	Residue		Distance (Å)		Atom	Residue		Distance (Å)
W71	O	Gly *A*	25	2.84	W66	O	Gly *B*	25	3.08
	O	Ile *A*	102	3.36		O	Ile *B*	102	2.70
	O	Ser *A*	100	2.76		OH	W	70	2.95
						OH	W	233	2.80
W49	N	Val *A*	146	2.97	W67	N	Val *B*	146	3.03
	OH	W	56	2.92		OH	W	116	2.79
	OH	W	2	3.45		OH	W	100	3.07
	OH	W	67	3.28		OH	W	49	3.28
	OH	W	100	2.74		OH	W	145	2.70
W55	O	His *A*	69	2.62	W69	O	His *B*	69	2.66
	O	Asp *A*	76	2.95		O	Asp *B*	76	2.98
	OH	W	107	2.91		OH	W	139	2.95
	OH	W	146	2.47		OH	W	228	2.57
W89	OG1	Thr *A*	37	3.10	W74	OG1	Thr *B*	37	3.24
	O	Glu *A*	119	2.91		O	Glu *B*	119	2.92
	OH	W	31	2.82		OH	W	241	2.76
	OH	W	226	3.17		OH	W	34	2.86
W42	OD2	Asp *A*	74	2.65	W76	OD2	Asp *B*	74	2.72
	O	Leu *A*	124	2.72		O	Leu *B*	124	2.72
	OH	W	301	3.30		NZ	Lys *B*	126	2.62
						OH	W	216	2.55
W87	OG	Ser *A*	109	2.73	W79	OG	Ser *B*	109	2.78
	OH	W	81	3.11		OH	W	45	3.49
	OH	W	236	2.77		OH	W	236	2.72
	OH	W	57	3.34		OH	W	85	3.12
W81	O	Leu *A*	104	2.77	W85	O	Leu *B*	104	2.74
	OH	Tyr *A*	149	2.73		OH	Tyr *B*	149	2.88
	OH	W	87	3.11		OH	W	79	3.12
	OH	W	267	3.21					
W155	N	Gly *A*	12	2.92	W101	N	Gly *B*	12	2.88
	N	Gly *A*	12	2.92		N	Val *B*	14	3.31
	O	Leu *A*	142	2.74		O	Leu *B*	142	2.67
	OH	W	289	3.00					
W113†	OG1	Thr *A*	37	2.65	W114†	OG1	Thr *B*	37	2.89
	O	Asp *A*	38	2.67		O	Asp *B*	38	2.72
	OH	W	187	3.03		OH	W	161	3.33
						OH	W	141	2.72
						OH	W	297	2.65
W125	O	Leu *A*	82	2.60	W90	O	Leu *B*	82	2.76
	O	Asn *A*	84	3.34		O	Asn *B*	84	3.04
	OH	W	294	2.89		OH	W	127	2.74
	OH	W	188	3.39		OH	W	121	2.81
W187	O	Leu *A*	40	2.44	W141	O	Leu *B*	40	2.60
	OH	W	113	3.03		OH	W	114	2.72
	OH	W	83	3.16		OH	W	136	3.11
	OH	W	115	3.35		OH	W	297	2.66
W144	O	Ala *A*	4	3.03	W162	O	Ala *B*	4	3.02
	ND1	His *A*	19	2.71		ND1	His *B*	19	3.19
	OG	Ser *A*	150	3.11		OG	Ser *B*	150	3.41
	OH	W	240	3.14		OH	W	203	2.70
	OH	W	334	2.87					

* Deviation 0.39 Å. † Deviation 0.43 Å, solvent exposed area 16/21 Å^2.

r.m.s. deviation (0.359 Å) observed for the Cα positions overlay of subunits *A* and *B*. Among these, 25 pairs, listed in Table 6 along with their hydrogen-bonding interactions, have a solvent-accessible area less than 3 Å^2, and, on the basis of their structural role, can be clustered in the following classes: (i) belonging to the active-site channel; (ii) stabilizing the 63–78 segment of loop IV; (iii) at the dimer interface cleft; (iv) at the upper end of the β-barrel; (v) in the five-residue turn connecting β-strands 1*a* and 2*b* to the N-terminal part of β-strand 8*h*; (vi) sparse solvent having a structural role, but not forming a connected group.

Classes (i), (ii), (iii) and (iv) will be discussed in detail, while class (v) has already been dealt with in the previous section.

(i) The water molecules located in the active-site channel form a well defined hydrogen-bonded network which starts from the copper-liganding solvent

molecules W38 and W10 (in subunits *A* and *B*, respectively), and extends in two opposite directions (Fig. 5). On one side, W21 and W25 (in subunits *A* and *B*, respectively) interact with W13 and W11, that in turn hydrogen bond the peptide N atom of the copper and zinc-liganding residue His61 as well as to carbonyl O atom of the electrostaticaly important residues Lys134 in both subunits (Getzoff *et al.*, 1983; Polticelli *et al.*, 1994, 1995, 1996). Thus, the conformation of the active-site channel, and in particular the appropriate mutual distances of the catalytically important residues are regulated not only by intra-protein but also by solvent–protein interactions. The second branch of hydrogen-bonded interactions is directed towards residues Gly139, which interact through their carbonyl O atom with W32 and W30 (in subunits *A* and *B*, respectively).

Two additional solvent molecule pairs (W177 and W168, and W153 and W317, in subunits *A* and *B*, respectively) have been located at sites differing by 2 r.m.s. deviations in both subunits (0.718 Å); together with the side chain of Arg141 they are mostly responsible for inaccesibility of the active-site centre. Among these, W177 and W168 hydrogen bond to the carbonyl O atom of Gly139, as well as to the Arg141 NE atom, contributing to the Arg141 side-chain orientation. A remarkably similar solvent organization in the active-site channel has been observed in the BCo-SOD and Y-SOD structures (Djinović, Coda *et al.*, 1992; Djinović, Gatti *et al.*, 1992), which display quite comparable catalytic constants (O'Neill *et al.*, 1988), suggesting a role of active-site solvent structure in promoting the functional properties of the enzyme.

(ii) The C-terminal part of loop IV (residues 60–80) hosts all four zinc-liganding residues. This region does not adopt a defined secondary structure, its conformation being stabilized by main-chain to main-chain, side-chain to side-chain hydrogen bonds as well as by conserved solvent–protein interactions. Three water molecules in each subunit, W3 and W6, W12 and W14, and W55 and W69 (in subunits *A* and *B*, respectively) coincide within 0.39 Å when their positions in subunits *A* and *B* are compared. W3 bonds to main-chain N atoms of residues Glu65 and Val79, being at the two ends of the loop IV region, as well as to W12 and W14 (in subunits *A* and *B*, respectively) and the Asn63 OD1 atom. Residue 63 is conserved as Asn in all eukaryotic SOD's, and hosts an Asp in all but one of the known prokaryotic enzymes (Bordo *et al.*, 1994). Similarly, W55 and W69 solvent molecules interact with the carbonyl O atoms of residues His69 and Asp76, the former one also being a zinc-liganding residue, while W12 and W14 hydrogen bond to Arg99 O and to W99 and W53 (in subunits *A* and *B*, respectively).

(iii) In an analysis of high-resolution crystal structures Kuhn *et al.* (1992) noticed, that the solvent molecules are three times more likely to be in grooves than on a flat or convex surface of the protein and, moreover, that water molecules in grooves discriminate considerably more between polar and non-polar groups. In this respect, the solvent molecules located in the X-SOD*b* dimer cleft show a conserved pattern formed by specific hydrogen-bonding interactions. Part of these, namely those between Tyr149 and solvent molecules W45 and W57, have already been discussed in *X-SOD isoenzymes and dimer stability*. The hydrogen-bonding network in the cleft between the two X-SOD*b* subunits is centered on the completely buried W236 molecule, approximately located on the molecular twofold axis (Fig. 4). The hydrogen bonds extend along the groove, through solvent molecules related by the local twofold symmetry W45 and W57, and W87 and W79 interacting with the Ile111 O and Ser109 OG atoms, as well as with water molecules W81 and W85 which in turn contact Leu104 O and Tyr149 OH atoms. An additional solvent molecule W24 and W16 (in subunits *A* and *B*, respectively), has been located, binding to Arg113 NH1, and carbonyl O atoms of residues Pro107 and Ser109, determining in this way the Arg113 side-chain orientation in a position suitable for interaction with residue Tyr149. The inter-subunit interactions are therefore defined not only by finely tuned enzyme surfaces forming the dimer contact area, but also by conserved and balanced solvent structure.

(iv) The upper end of the SOD β-barrel is formed by three loop regions, namely loop I, loop III and N-terminal part of the loop VII. The completely buried Leu36 acts as a cork to this end of the β-barrel, closing it by means of a number of conserved hydrophobic interactions in the protein core. Additionally, solvent molecules located in the groove formed by residues 36–40 and 118–121 contribute to an efficient sealing of the β-barrel. A chain of five water molecules (W31 and W34, W89 and W74, W113 and W114, W187 and W141, and W83 and W43) hydrogen bonded to main-chain and/or side-chain atoms of residues Tyr37, Asp38, Leu40, Glu119 can be observed (see Table 6).

4.6. *Crystal contacts*

The high-resolution diffraction of the X-SOD*b* crystals may be in part due to the high number of crystal contacts (27). The residues in the two polypeptide chains involved in intermolecular side-chain–side-chain, side-chain–main-chain and even main-chain–main-chain interactions belong to the solvent exposed β-turn or loop regions. Of particular interest is the formation of a short antiparallel intermolecular two stranded β-sheet between the electrostatic loop VII residues Gly128, Asn129, Glu130 of subunit *A* and the same residues of a symmetry-related subunit *B*. Among these, residue 129 adopts an extended main-chain conformation, while residues 128 and 130 are in left-handed α-helical

and right-handed α-helical conformations, respectively. The Cα positions of the residues involved in these main-chain–main-chain hydrogen-bonded contacts are little affected by such interactions, their main-chain displacements being below the 0.36 Å Cα r.m.s. deviation obtained after superposition of two X-SOD*b* subunits.

The alternate conformation of Ser60 in subunit *A* is stabilized by hydrogen bonds to the carboxylate group of Glu88 from a symmetry-related subunit *A*, while Ser60 from subunit *B* is not involved in intermolecular contacts and shows only one side chain conformation. Residue Glu88, in subunit *B*, forms a salt bridge with the basic guanidinium group of a symmetry-related Arg141, the most important residue for substrate attraction and orientation in the active-site pocket. The guanidinium group of Arg141 is at 6.81 and 7.06 Å (in subunits *A* and *B*, respectively) from the Cu^{2+} center, similar to what is observed in the BCo-SOD and Y-SOD crystal structures (Djinović, Coda *et al.*, 1992; Djinović, Gatti *et al.*, 1992). Despite the salt bridge, the side-chain conformation of Arg141 is almost identical in the two crystallographically independent X-SOD*b* subunits, the orientation of the side chain being defined by strong hydrogen bonds between Arg141 atoms NH1 and NH2 and carbonyl O atoms of residues Cys55 and Gly59. Comparison with the observed Arg141 side-chain conformation in the crystal structure of X-SOD*b*:CN again shows that this residue conformation is highly preserved upon anion binding as well as upon salt-bridge formation with residue Glu88. In addition, the cyanide anion sites in the two crystallographically independent subunuits are equally occupied and structurally identical regardless of the Arg141–Glu88 intermolecular interaction, which is present only in the active-site channel of the *B* subunit (Djinović Carugo *et al.*, 1994). This observation suggests that a secondary role of residue Arg141 could be that of trapping or diverting bigger negatively charged species present in the cell cytoplasm, to maintain accessibility of the active-site channel for the substrate. The side chain of Glu88, on the other hand is clearly perturbed by the salt link, the maximum deviation between 88 OE1 atoms in the two subunits being 3.92 Å.

References

Argese, E., Viglino, P., Rotilio, G., Scarpa, M. & Rigo, A. (1987). *Biochemistry*, **26**, 3224–3228.

Arndt, U. W. & Wonacott, A. J. (1977). *The Rotation Method in Crystallography*. Amsterdam: North-Holland.

Banci, L., Bertini, I., Bruni, B., Carloni, P., Luchinat, C., Mangani, S., Orioli, P., Piccioli, M., Ripniewski, W. & Wilson, K. S. (1994). *Biochem. Biophys. Res. Commun.* **202**, 1088–1095.

Banci, L., Bertini, I., Luchinat, C., Monnani, R. & Scozzafava, A. (1988). *Inorg. Chem.* **27**, 107–109.

Bannister, W. H., Bannister, J., Barra, D., Bond, J. & Bossa, F. (1991). *Free Rad. Res. Commun.* **12–13**, 349–361.

Battistoni, A., Carrì, M. T., Mazzetti, P. & Rotilio, G. (1992). *Biochem. Biophys. Res. Commun.* **186**, 1339–1344.

Beyer, W. F., Fridovich, I., Mullenbach, G. T. & Hallewell, R. A. (1987). *J. Biol. Chem.* **262**, 11182–11187.

Bisbee, A., Beaker, M. A., Wilson, A. C., Hadji-Azini, I. & Fishberg, M. (1977). *Science*, **195**, 785–787.

Blackburn, N. J., Strange, R. W., McFadden, L. M. & Hasnain, S. S. (1987). *J. Am. Chem. Soc.* **109**, 7162–7170.

Bordo, D., Djinović, K. & Bolognesi, M. (1994). *J. Mol. Biol.* **238**, 366–386.

Brünger, A. T. (1992*a*). *X-PLOR Manual*. Version 3.0. Yale University, New Haven, CT, USA.

Brünger, A. T. (1992*b*). *Nature (London)*, **355**, 472–475.

Capo, C. R., Polticelli, F., Calabrese, L., Schininà, M. E., Carrì, M. T. & Rotilio, G. (1990). *Biochem. Biophys. Res. Commun.* **173**, 1186–1193.

Collaborative Computational Project, Number 4 (1994). *Acta Cryst.* D**50**, 760–763.

Cudd, A. & Fridovich, I. (1982). *J. Biol. Chem.* **257**, 11443–11447.

Desideri, A., Falconi, M., Polticelli, F., Bolognesi, M., Djinović, K. & Rotilio, G. (1992). *J. Mol. Biol.* **223**, 337–342.

Djinović, K., Coda, A., Antolini, L., Pelosi, G., Desideri, A., Falconi, M., Rotilio, G. & Bolognesi, M. (1992). *J. Mol. Biol.* **226**, 227–238.

Djinović, K., Gatti, G., Coda, A., Antolini, L., Pelosi, G., Desideri, A., Falconi, M., Marmocchi, F., Rotilio, G. & Bolognesi, M. (1992). *J. Mol. Biol.* **225**, 791–809.

Djinović Carugo, K., Battistoni, A., Carrì, M. T., Polticelli, F., Desideri, A., Rotilio, G., Coda, A. & Bolognesi, M. (1994). *FEBS Lett.* **349**, 93–98.

Djinović Carugo, K., Collyer, C., Coda, A., Carrì, M. T., Battistoni, A., Bottaro, G., Polticelli, F., Desideri, A. & Bolognesi, M. (1993). *Biochem. Biophys. Res. Commun.* **194**, 1008–1011.

Engh, R. A. & Huber, R. (1991). *Acta Cryst.* A**47**, 392–400.

Fielden, E. M., Roberts, P. B., Bray, R. C., Lowe, D. J., Mautner, G. N., Rotilio, G. & Calabrese, L. (1974). *Biochem. J.* **139**, 49–60.

Fisher, C. L., Tainer, J. A., Pique, M. E. & Getzoff, E. D. (1990). *J. Mol. Graphics*, **8**, 125–132.

French, S. & Wilson, K. S. (1978). *Acta Cryst.* A**34**, 517–525.

Fridovich, I. (1986). *Adv. Enzymol.* **58**, 61–97.

Getzoff, E. D., Cabelli, D. E., Fisher, C. L., Parge, H. E., Viezzoli, M. S., Banci, L. & Hallewell, R. A. (1992). *Nature (London)*, **358**, 347–351.

Getzoff, E. D., Tainer, J. A., Stempien, M. M., Bell, G. I. & Hallewell, R. A. (1989). *Proteins*, **5**, 322–336.

Getzoff, E. D., Tainer, J. A., Weiner, P. K., Kollman, P. A., Richardson, J. & Richardson, D. C. (1983). *Nature (London)*, **306**, 287–290.

Halliwell, B. & Gutteridge, J. M. (1989). *Free Radicals in Biology and Medicine*, pp. 22–408. Oxford: Clarendon Press.

Hamilton, W. C. (1965). *Acta Cryst.* **18**, 502–510.

Hutchinson, E. G. & Thornton, J. M. (1993). *Protein Eng.* **6**, 233–245.

Jones, T. A. (1978). *J. Appl. Cryst.* **11**, 268–272.

Kabsch, W. & Sander, C. (1983). *Biopolymers*, **22**, 2577–2637.

Kitagawa, Y., Tanaka, N., Hata, Y., Kusonoki, M., Lee, G., Katsube, Y., Asada, K., Aibara, S. & Morita, Y. (1991). *J. Biochem.* **109**, 447–485.

Konnert, J. H. & Hendrickson, W. A. (1980). *Acta Cryst.* A**36**, 344–350.

Kuhn, L. A., Siani, M. A., Pique, M. E., Fisher, C. L., Getzoff, E. D. & Tainer, J. A. (1992). *J. Mol. Biol.* **202**, 637–657.

Lamzin, V. S. & Wilson, K. S. (1993). *Acta Cryst.* D**49**, 129–147.
Laskowski, R. A., MacArthur, M. W., Moss, D. S. & Thornton, J. M. (1993). *J. Appl. Cryst.* **26**, 282–291.
Lepock, J. R., Frey, H. E. & Hallewell, R. A. (1990). *J. Biol. Chem.* **265**, 21612–21618.
Leslie, A. G. W. (1986). *Daresbury Lab. Inf. Q. Prog. Crystallogr.* Vol. 18, pp. 33–39. Warrington, England: Daresbury Laboratory.
McRee, D. E., Redford, S., Getzoff, E., Lepock, J. R., Hallewell, R. A. & Tainer, J. (1990). *J. Biol. Chem.* **244**, 14234–14241.
Matthews, B. W. (1968). *J. Mol. Biol.* **33**, 491–497.
O'Neill, P., Davies, S., Fielden, E. M., Calabrese, L., Capo, C., Marmocchi, F., Natoli, G. & Rotilio, G. (1988). *Biochem. J.* **251**, 41–46.
Orpen, A. G., Brammer, L., Allen, F. H., Kennard, O., Watson, D. & Taylor, R. (1989). *J. Chem. Soc. Dalton Trans.* pp. S1–S83.
Parge, H. E., Hallewell, R. A. & Tainer, J. A. (1992). *Proc. Natl Acad. Sci. USA*, **89**, 6109–6113.
Parker, M. W. & Blake, C. C. F. (1988). *J. Mol. Biol.* **199**, 649–661.
Polticelli, F., Battistoni, A., Bottaro, G., Carrì, M. T., O'Neill, P., Desideri, A. & Rotilio, G. (1996). *FEBS Lett.* In the press.
Polticelli, F., Bottaro, G., Battistoni, A., Carrì, M. T., Djinović Carugo, K., Bolognesi, M., O'Neill, P., Rotilio, G. & Desideri, F. (1995). *Biochemistry*, 6034–6049.
Polticelli, F., Falconi, M., O'Neill, P., Petruzzelli, R., Galtieri, A., Lania, A., Calabrese, L., Rotilio, G. & Desideri, A. (1994). *Arch. Biochem. Biophys.* **312**, 22–30.
Priestle, J. P. (1988). *J. Appl. Cryst.* **21**, 572–576.
Ramakrishnan, C. & Ramachandran, G. N. (1965). *Biophys. J.* **5**, 909–933.
Read, R. J. (1986). *Acta Cryst.* A**42**, 140–149.
Roe, J. A., Butler, A., Scholler, D. M., Valentine, J. S., Marky, L. & Breslauer, K. J. (1988). *Biochemistry*, **27**, 950–958.
Schininà, M. E., Barra, D., Bossa, F., Calabrese, L., Montesaro, L., Carrì, M. T., Matiottini, P., Amaldi, F. & Rotilio, G. (1989). *Arch. Bioch. Biophys.* **272**, 507–515.
Sergi, A., Ferrario, M., Polticelli, F., O'Neill, P. & Desideri, A. (1996). *J. Phys. Chem.* In the press.
Sheldrick, G. M. (1993). *SHELXL*93. University of Göttingen, Germany.
Simurda, M. C., van Keulen, H., Rekosh, D. M. & Lo Verde, P. T. (1988). *Exp. Parasitol.* **67**, 73–84.
Sines, J. J., Allison, S. A. & McCammon, J. A. (1990). *Biochemistry*, **29**, 9403–9412.
Stallings, W. C., Pattridge, K. A., Strong, R. K., Ludwig, M. L., Yamakura, F., Isobe, T. & Steinman, H. M. (1987). *Active Site Homology in Iron and Manganese Superoxide Dismutase*, in *Patterson and Pattersons*, edited by J. P. Glusker, B. K. Patterson & M. Rossi, pp. 505–513. Oxford University Press.
Stellwagen, E. & Wilgus, H. (1978). *Biochemistry of Thermophyl*, edited by S. Friedman, pp. 223–232. Orlando: Academic Press.
Tainer, J. A., Getzoff, E. D., Beem, K. M., Richardson, J. S. & Richardson, D. C. (1982). *J. Mol. Biol.* **160**, 181–217.
Tegelstrom, H. (1975). *Hereditas*, **81**, 185–198.
Tilton, R. F., Dewan, J. C. & Petsko, G. A. (1992). *Biochemistry*, **31**, 2469–2481.